



Cite this: *Nanoscale*, 2017, 9, 13214

Oxygen defect engineering by the current effect assisted with temperature cycling in a perovskite-type $\text{La}_{0.7}\text{Sr}_{0.3}\text{CoO}_3$ film†

J. Li,^{a,b} J. Wang,^{*a,b} H. Kuang,^{a,b} H. R. Zhang,^{a,b} Y. Y. Zhao,^a K. M. Qiao,^{a,b} F. Wang,^c W. Liu,^c W. Wang,^{a,b} L. C. Peng,^{a,b} Y. Zhang,^{a,b} R. C. Yu,^{a,b} F. X. Hu,^{id *a,b} J. R. Sun^{id a,b} and B. G. Shen^{a,b}

Introducing and modulating the oxygen deficiency concentration have been received as an effective way to obtain high catalytic activity in perovskite oxides. However, it is difficult to control the oxygen vacancy in conventional oxygen defect engineering due to harsh reaction conditions at elevated temperatures and the reducing atmosphere, which make it impractical for many technological applications. Herein, we report a new approach to oxygen defect engineering based on the combination of the current effect and temperature cycling at low temperature. Our investigations revealed that the electrical conductivity of the (011)- $\text{La}_{0.7}\text{Sr}_{0.3}\text{CoO}_3/\text{PMN-PT}$ film changes continuously from metallicity to insulativity under repeated transport measurements below room temperature, which indicates the transformation of the Co^{4+} state to Co^{3+} in the film. Further experiments and analysis revealed that oxygen vacancies can be well regulated by the combined current effect and temperature cycling in repeated measurements, which results in a decrease of $\text{Co}^{4+}/\text{Co}^{3+}$ and thus the remarkable variation of conductive properties of the film. Our work provides a simple and highly efficient method to engineer oxygen vacancies in perovskite-type oxides and brings new opportunities in designing high-efficiency oxidation catalysts.

Received 4th May 2017,
Accepted 4th August 2017

DOI: 10.1039/c7nr03162a

rsc.li/nanoscale

Introduction

Multivalent transition metal oxides have attracted significant interest due to their intriguing physical properties based on the flexibility of transition metal charge states. In particular, oxygen-deficient perovskite oxides have received considerable attention due to their unique mixed electronic and ionic conducting properties, which make them appealing in a wide range of applications such as oxidation catalysts, gas sensors, oxygen separation membranes and electrode materials for solid oxide fuel cells.^{1–4} It was previously believed that the catalytic activity is strongly associated with the binding strength of oxygen molecules and surface redox-active sites according to the so-called Sabatier's principle. However, recent

studies indicate that the surface redox center at transition metal cations cannot fully explain the catalytic behavior in oxygen-deficient perovskite oxides.^{5–8} Further experimental and theoretical studies correlated oxygen electrocatalysis with the electronic structure of oxygen and metal cations such as e_g band filling of transition metal ions, the O p-band center position relative to the Fermi level and hybridization of the metal-3d and O-2p orbitals.^{9–11} These studies provide a promising strategy to achieve highly active oxide catalysts through controlling the electronic structure of perovskite oxides. Moreover, experiments have revealed that the oxygen vacancies not only affect the electronic state between the metal-3d and O-2p but also change the metal cation valence, leading to regulation of the electronic structure of perovskite oxides.^{6,9,12} As a result, oxygen defect engineering is accepted as an efficient way to obtain high catalytic activity in perovskite oxides.

Perovskite-type oxides, $\text{La}_{1-x}\text{Sr}_x\text{CoO}_{3-\delta}$, have been viewed as an excellent platform for the study of reversible redox activity due to their characteristic properties of high oxygen ionic diffusivity, high electrical conductivity and high oxygen off stoichiometry.^{12–16} It has been found that the substitution of Sr^{2+} for La^{3+} changes Co^{3+} into Co^{4+} in $\text{La}_{1-x}\text{Sr}_x\text{CoO}_3$ systems, resulting in the mixing valences Co irons.¹⁷ As x increases, double exchange (DE) interaction in the $\text{La}_{1-x}\text{Sr}_x\text{CoO}_3$ system

^aBeijing National Laboratory for Condensed Matter Physics and State Key Laboratory of Magnetism, Institute of Physics, Chinese Academy of Sciences, Beijing 100190, P. R. China. E-mail: wangjing@iphy.ac.cn, fxhu@iphy.ac.cn

^bSchool of Physical Sciences, University of Chinese Academy of Sciences, Beijing 100049, P. R. China

^cShenyang National Laboratory for Materials Science, Institute of Metal Research, Chinese Academy of Sciences, 72 Wenhua Road, Shenyang 110016, P. R. China

†Electronic supplementary information (ESI) available. See DOI: 10.1039/c7nr03162a

becomes stronger and the $\text{La}_{1-x}\text{Sr}_x\text{CoO}_3$ system undergoes an insulator-to-metal transition. However, the high energy of the Co^{4+} valence state promotes its conversion to the more stable Co^{3+} or/and Co^{2+} states, leaving oxygen vacancies in the CoO_6 octahedron. As oxygen vacancies increase in the $\text{La}_{1-x}\text{Sr}_x\text{CoO}_3$ film, the ferromagnetism becomes weaker¹⁸ and the transport mechanism is transformed from the DE interaction effect to variable range hopping (VRH), characterized by the enhancement of overall resistivity and the emergence of insulativity.¹⁹ More importantly, experiments revealed that the formation of oxygen vacancies from oxygen off stoichiometry, which is usually realized by annealing in a reducing atmosphere, greatly affects the redox activity of $\text{La}_{1-x}\text{Sr}_x\text{CoO}_{3-\delta}$.^{9,20} However, the possibility of a reversible redox reaction and the associated property changes of $\text{La}_{1-x}\text{Sr}_x\text{CoO}_{3-\delta}$ have not been systematically studied owing to the difficulty in precisely controlling the oxygen defect concentration. Although oxygen deficiency can be induced by growth or annealing in a reducing atmosphere, the strong redox property and narrow control range makes it difficult to regulate the oxygen defect structure of $\text{La}_{1-x}\text{Sr}_x\text{CoO}_{3-\delta}$ actively. Moreover, experiments showed that the formation of oxygen off-stoichiometric phases in perovskite-type oxides usually requires a very high annealing temperature and long annealing time,^{21–24} which are impractical for many technological applications.

In this work, we revealed a low cost and highly efficient method to engineer oxygen defects in $\text{La}_{0.7}\text{Sr}_{0.3}\text{CoO}_3$ (LSCO) film by the application of an electric current and temperature cycling below room temperature. Investigations of the magnetic and transport properties in the (011)-oriented LSCO film demonstrate that the combined current effect and temperature cycling in the repeated temperature-dependent transport measurements could drive a continuous transformation of electrical conductivity from metallicity to insulativity by introducing oxygen vacancies and reducing the content of cation Co^{4+} in the film. Our work provides a novel and practical method to manufacture extra oxygen defects and regulate the concentration of oxygen vacancies in the LSCO thin film through adjusting the combination of the current effect and temperature cycling, and brings new opportunities in preparing high-efficiency solid oxidation catalysts.

Experimental

The 50 nm $\text{La}_{0.7}\text{Sr}_{0.3}\text{CoO}_3$ (LSCO) films were grown on the (011)-oriented $\text{Pb}(\text{Mg}_{1/3}\text{Nb}_{2/3})_{0.7}\text{Ti}_{0.3}\text{O}_3$ (PMN-PT) single crystalline substrate with a dimension of $3 \times 5 \text{ mm}^2$ by the pulsed laser deposition (PLD) technique. The pulsed laser (KrF 248 nm) with a pulse energy of 290 mJ and a repetition rate of 3 Hz was used to ablate the stoichiometric target, which was prepared by the conventional solid reaction method. During the deposition process, the temperature of the substrate was kept at 740 °C and the oxygen pressure was kept at 1 Pa. The film was subsequently cooled down at the same oxygen pressure after deposition. The lattice structure of the LSCO

film was checked by X-ray diffraction (XRD) and reciprocal space maps (RSM) using $\text{Cu K}\alpha$ radiation ($\lambda = 1.5406 \text{ \AA}$) on a Bruker AXS D8-Discover. The magnetic properties of the LSCO film were characterized using the Quantum Design superconducting quantum interference device-vibrating sample magnetometer (SQUID-VSM). The measurement of the electrical transport properties was performed by a Keithley 2601 Sourcemeter and a 2182 nanovoltmeter. A current of 1 μA was applied for each measuring temperature point during temperature cycling. The duration of the applied current at each measuring point is 1 s. During the measurement of electrical transport properties, SQUID-VSM provides a controlled temperature environment at a range between 20 K and 320 K. X-ray absorption spectroscopy (XAS) measurements in total electron yield mode were carried out to check the variation in the electronic structure of the film at Beamline BL08U1A of Shanghai Synchrotron Radiation Facility. All spectra were collected at a normal incidence of radiation with respect to the film surface. The energy resolution of the absorption spectra was set to 0.3 eV.

Results and discussion

The θ - 2θ X-ray diffraction patterns of the LSCO film on the PMN-PT substrate are shown in Fig. 1(a). The result indicates

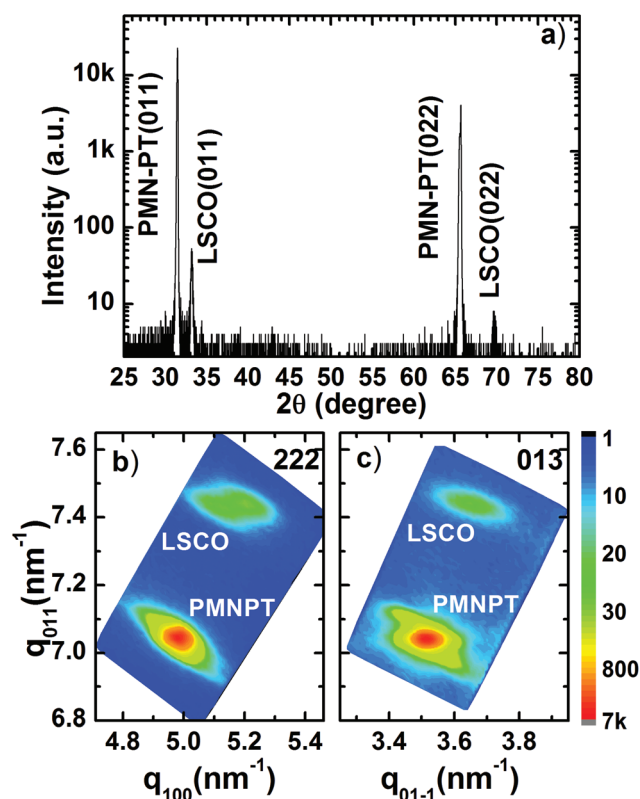


Fig. 1 (a) θ - 2θ X-ray diffraction patterns of 50 nm (011)-LSCO/PMN-PT film. (b) & (c) XRD reciprocal space maps around (222) (b) and (013) (c) reflections for the same LSCO film on the PMN-PT substrate.

that the LSCO/PMN-PT film is highly oriented along the [011] direction and the out-of-plane lattice constant is calculated to be 2.694 Å. Compared with bulk LSCO ($a \sim 3.82$ Å),²⁵ the film undergoes an out-of-plane compressive strain which was calculated to be -0.25% along the [011] direction by using the equation $\epsilon_{[011]} = (d_{\text{film}} - d_{\text{bulk}})/d_{\text{bulk}}$. Fig. 1(b) and (c) show the X-ray reciprocal space maps collected around (222) and (013) reflections of the LSCO/PMN-PT film, respectively. By analyzing the two RSM patterns, we could obtain the lattice parameters and thus the strains along both orthogonal [100] and [01-1] directions in the deposition plane. The lattice constants of the film are determined to be 3.93 Å and 2.74 Å along the in-plane [100] and [01-1] directions, respectively. Accordingly, the in-plane strain $\epsilon_{[100]}$ and $\epsilon_{[01-1]}$ are calculated as 2.88% and 1.48%, respectively. The results show that the LSCO/PMN-PT film undergoes different tensile strain along [100] and [01-1] directions. Such anisotropic in-plane lattice strain would bring about a different overlap of O 2p and Co 3d electronic orbitals along [100] and [01-1], resulting in the in-plane anisotropy of the magnetic and transport properties.

Fig. 2(a) presents the temperature-dependent magnetization under a 500 Oe magnetic field along the in-plane [100] (open point) and [01-1] (solid point) directions after 500 Oe field cooling (FC) from room temperature. It is found that the Curie temperature (T_C) of the film, determined from both curves (215 K for [100] direction and 217 K for [01-1]), is a little bit lower than the bulk but similar to previous reports.^{26,27} It is noteworthy that the difference in T_C for the two directions suggests relatively weak magnetism in the [100] direction. Fig. 2(b) shows the magnetic hysteresis loops of LSCO/PMN-PT at 10 K along both in-plane directions. The image indicates that the LSCO/PMN-PT film is in a ferromagnetic state at 10 K, which is in coincidence with previous reports.^{18,26,28} Meanwhile, the better squareness of the loop and the higher remnant magnetic moment along the [01-1] direction indicate that the magnetic moment prefers to align in the [01-1] direction. These results demonstrate a clear in-plane magnetic anisotropy in the LSCO/PMN-PT film, which should be ascribed

to the anisotropic lattice strain field induced by the substrate. Actually, the larger strain at the [100] direction leads to weaker hybridization between the neighboring $\text{Co}^{3+}/\text{Co}^{4+}$ 3d orbital and O^{2-} 2p orbital, resulting in a suppression of the DE interaction²⁹ and thus weak magnetism as shown in Fig. 2. The resistance along the in-plane [100] and [01-1] directions at a temperature range between 320 K and 20 K are also plotted in Fig. 2(a). It is seen that the resistance along both directions exhibit a metallic temperature dependence in a temperature interval below T_C , but insulating behavior outside the interval. At the bottom and top of the interval, two metal-insulator transitions are identified (see the Fig. 2(a)). The transition temperature at the top of the interval, T_{MI1} (211 K for both directions), is consistent with T_C , indicating that the metallic conduction is related to the DE interaction.^{17,19,28} Meanwhile, the transition temperature at the bottom of the interval (T_{MI2}) in the [01-1] direction is lower than the one in the [100] direction, which is ascribed to the stronger DE effect caused by the smaller tensile strain at the [01-1] direction.

The stability of the Co^{4+} state was further investigated by repeatedly measuring the resistance of the LSCO film at a temperature range between 320 K and 20 K. A series of curves for two in-plane directions are plotted in Fig. 3(a) and (b). It is surprising to find that the transport characteristics of the LSCO film change steadily from metallicity to insulativity with the cycle number of measurements. The overall resistance is enhanced by the repeated measurements. Moreover, the metal-insulator transition at high temperature, which is relating to the change of magnetic order, shifts to lower temperature gradually with the cycle number of measurements. Further increases in the cycle number makes this metal-insulator transition gradually vanish. Meanwhile, in accordance with the variation of T_{MI1} , the transition at low temperature moves towards high temperature with the increase of cycle number, suggesting the development of insulating conduction. Fig. 4(a) plots the summary of T_{MI1} and T_{MI2} for both in-plane directions against the cycle number of repeated measurements. In the beginning of the repeated measure-

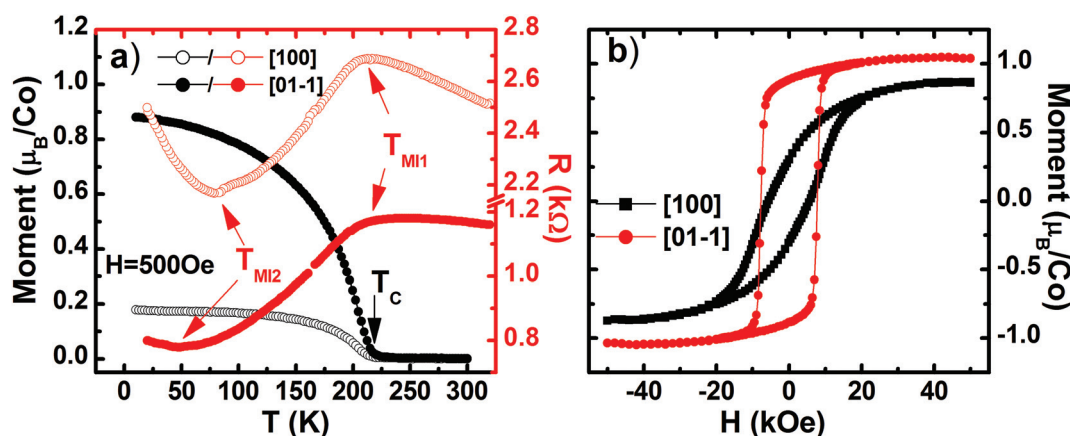


Fig. 2 (a) Temperature-dependent magnetization under a 500 Oe field (left axis, black) and resistance (right axis, red) in field cooling mode along both in-plane directions. (b) The magnetic hysteresis loops of LSCO/PMN-PT at 10 K along the in-plane [100] (black) and [01-1] (red) directions.

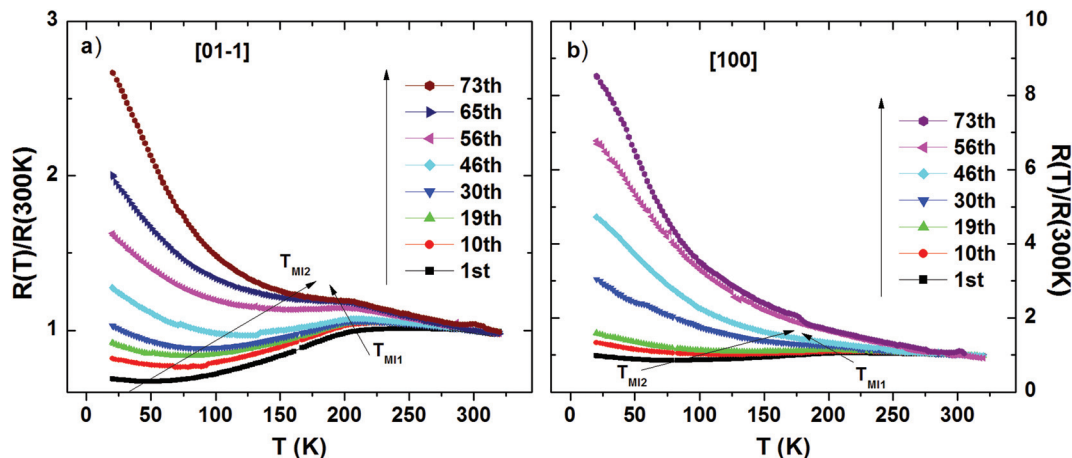


Fig. 3 Repeated temperature-dependent resistance measurements of the LSCO/PMN-PT film with a current of 1 μ A applied along [01–1] (a) and [100] (b) directions. The numbers in the images represent the cycle index of measurements.

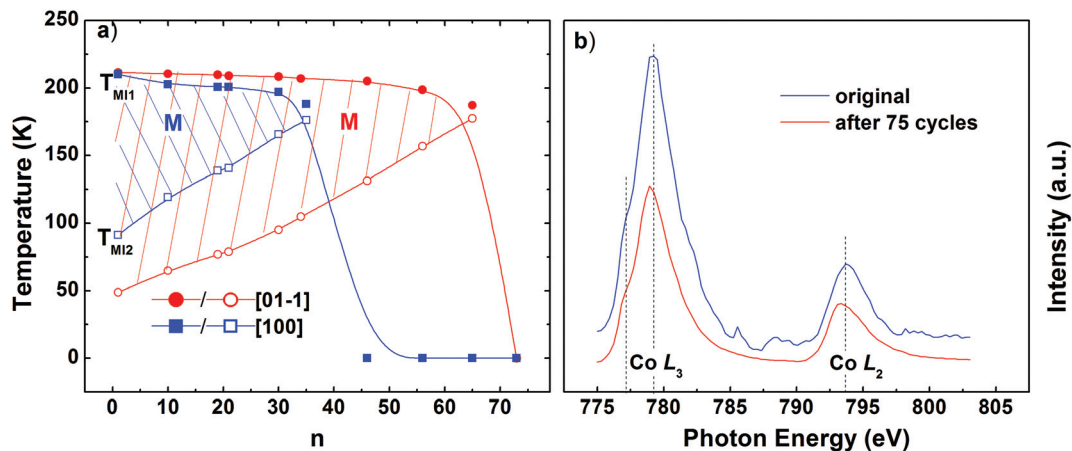


Fig. 4 (a) A summary for T_{MI1} and T_{MI2} as a function of cycle number of repeated transport measurements, n . The red solid (open) points represent T_{MI1} (T_{MI2}) for the [01–1] direction, and the blue ones for the [100] direction. The shadow regions indicate the metallic conduction area for both directions (blue for [100] and red for [01–1], respectively). (b) Co L-edge X-ray adsorption spectra for the LSCO film before and after repeated transport measurements.

ments, T_{MI1} decreases slightly and linearly with the cycle number, n , at both directions. Meanwhile, T_{MI2} increases continuously with n , moving close to T_{MI1} . As a result, the metallic conduction area shrinks with the cycle number of measurements. Moreover, a sharp drop of T_{MI1} is observed after T_{MI2} approaches T_{MI1} , corresponding to the disappearance of both transitions and the predominance of insulating conduction in the whole temperature range. Such a remarkable variation of conductive properties indicates that the ratio of Co^{4+}/Co^{3+} , which is considered to be the determinative role in the electronic transport process, decreases continuously with the cycle number of repeated transport measurements. Previous research has revealed that the transformation of the Co^{4+} state to Co^{3+} in the LSCO system, either by reduction of Sr doping or incorporation of oxygen vacancies, will shift the resistive transition at T_{MI1} to lower temperatures, accompanied by an enhancement of the overall resistivity.^{19,30}

Our scanning electron microscopy and energy-dispersive X-ray spectra measurements (section I of ESI, Fig. S1†) demonstrate that no anomalous Sr cluster area appears in the surface of the film and the Sr distribution is nearly consistent with that of La and Co elements both before and after repeated transport measurements, which excludes the effect of the reduction in Sr doping. On the other hand, careful X-ray diffraction (XRD) experiments before and after repeated measurements exhibit no obvious change in the diffraction patterns, indicating that the possible structural change related to the variation in conductivity, if any, may locate in very small areas. Actually, our high-resolution transmission electron microscope experiments (section II of ESI, Fig. S2†) do observe a periodic oxygen vacancy ordering modulation in very small regions of the film after repeated transport measurements, suggesting the accumulation of oxygen vacancies in the local areas of the film. Meanwhile, soft X-ray absorption spectroscopy (XAS)

measurements at the Co L_{2-3} absorption thresholds were carried out at the Beamline BL08U1A of Shanghai Synchrotron Radiation Facility to further examine the electronic structures and the Co valence states³¹ in the LSCO film. The observed changes in the electronic structure of the LSCO film after repeated transport measurements strongly suggest variation in the Co valence state due to oxygen vacancy formation. Fig. 4(b) shows the comparison of the Co L-edge spectra at 300 K for the LSCO film before and after repeated transport measurements. First of all, a mixture of high-spin (HS) Co^{4+} , HS Co^{3+} and low-spin (LS) Co^{3+} in the sample both before and after repeated measurements is suggested by the spectral shape at both edges, which is consistent with previous results of the LSCO film.³² Moreover, it is evident that the Co L_{2-3} spectral weights shift toward lower photon energies after repeated transport measurements. Such a shift suggests a lower Co valence in the LSCO film after measurements, evidencing the changes in the Co valence state toward Co^{3+} .³¹⁻³⁵ Previous studies have revealed that the increase in the 3d-electron count would drive changes in the electrostatic energy at the Co site, leading to shifts of both the core level and the final state wave functions.^{34,36} Thus, one can conclude from these results that extra oxygen vacancies were introduced in the film due to the repeated transport measurements.

A comparison of the magnetic properties before and after repeated transport measurements were further investigated with a magnetic field applied along both in-plane directions. Fig. 5 shows the comparison of the magnetic hysteresis loops at 10 K and the temperature-dependent magnetization under 500 Oe (the insets). It can be seen that the Curie temperature remains almost unchanged for both in-plane [100] and [01–1] directions. Meanwhile, the shape of the loop remains unchanged despite the saturated moment exhibiting a small variation for both directions, which demonstrates that the magnetic anisotropy remains unchanged after repeated transport measurements. Such inconsistent variation of the magnetic and electrical transport properties after repeated

measurements indicates that the HS state remains during the transformation of Co^{4+} ions to Co^{3+} . Previous spectral research has shown that Co^{4+} ions induced by Sr-doping in the strained $\text{La}_{0.7}\text{Sr}_{0.3}\text{CoO}_3$ film prefers to have a HS configuration ($3t_{2g}2e_g$) due to the Jahn–Teller (JT) splitting of t_{2g} resulting from Sr-doping and epitaxial strain.^{32,33} This JT splitting of t_{2g} could be stabilized by the strong in-plane strain in the present LSCO/PMN-PT, resulting in the maintenance of the HS configuration in Co^{3+} ions.

Based on the above results, one could speculate, naturally, that the electric current applied during repeated measurements probably plays a key role in the presented unusual evolution of the electrical conductivity, which may introduce oxygen vacancies near the electrical channels in the LSCO/PMN-PT film, and thus reduces the content of Co^{4+} . Usually, considerable oxygen loss in the LSCO film occurs at temperatures higher than 470 K in a vacuum or in an air environment.^{19,37} Recent studies^{38,39} on the $\text{La}_{2/3}\text{Sr}_{1/3}\text{MnO}_3$ film have revealed that Joule heating by an applied voltage/current can temporarily raise the temperature of the manganite oxide film and modify the oxygen vacancies doping condition. Theoretical simulations and spectroscopic experiments³⁸ show that Joule heating by a current of $\sim 50 \mu\text{A}$ (produced by a short triangular voltage pulse with 0.1 s duration) can generate a temperature gradient with a maximum temperature of $>600 \text{K}$ around the electrical contact and result in an electro-thermal redistribution of oxygen vacancies, inducing the oxygen deficient brownmillerite phase in the $\text{La}_{2/3}\text{Sr}_{1/3}\text{MnO}_3$ thin film (in submicrometer level).³⁸ Considering the high oxygen ionic diffusivity and the instability of the Co^{4+} ions of LSCO, it is reasonable to expect the occurrence of a similar current effect in the present experiments, which may activate the formation of oxygen deficiencies around the current channel and increase the concentration of oxygen vacancy in the film. Moreover, the strong tensile strain in the present LSCO film can lower the formation energy of the oxygen vacancies, facilitating the accommodation of oxygen vacancies in the

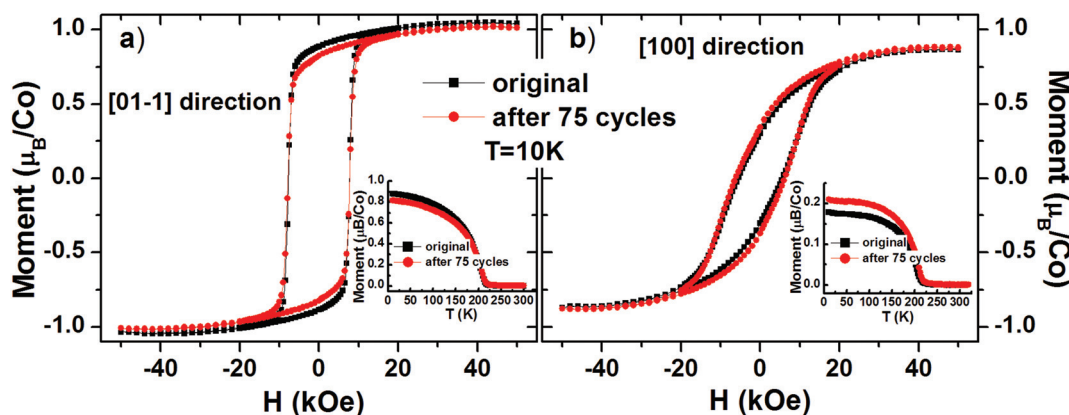


Fig. 5 The magnetic hysteresis loops of the LSCO/PMN-PT film at 10 K after repeated temperature-dependent resistance measurements (red) compared with the original one (black) along the in-plane [01–1] (a) and [100] (b) directions. The insets are the temperature-dependent moment under 500 Oe for the corresponding direction.

expanded lattice.^{40,41} Meanwhile, the electrical field produced by the measuring current may also activate the migration of oxygen vacancies by reducing the activation energy for oxygen vacancies migration in the LSCO film, and then promote the redistribution of oxygen vacancies. Thereby, the concurrent current-heating and electromigration can modify the concentration of the oxygen vacancy, decreasing the $\text{Co}^{4+}/\text{Co}^{3+}$ ratio in the film and thus leading to the increase of the overall resistance. Some experiments have shown strong evidence for the coexistence of ferromagnetic, metallic hole-rich clusters and insulating hole-poor matrix in Sr-doping $\text{La}_{1-x}\text{Sr}_x\text{CoO}_3$.^{25,29,32,42} At $x = 0.3$, the sufficiently large volume of the metallic hole-rich clusters leads to the percolation among hole-rich clusters, resulting in a ferromagnetic metallicity below T_C in the film thanks to the DE interaction between HS Co^{4+} and HS Co^{3+} ions.^{32,33,43} With the incorporation of oxygen vacancies by the combined current effect and temperature cycling, the ferromagnetic DE interaction between hole-rich clusters is weakened and a break-up of percolation occurs as the region of hole-rich clusters shrinks by a transformation of HS Co^{4+} to HS Co^{3+} , leading to the localization of the HS configurations in the hole-poor matrix. Instead, the hole-rich clusters couple ferromagnetically *via* superexchange interaction through the hole-poor matrix,²⁵ resulting in a ferromagnetic insulating state with small variation of magnetization. Such ferromagnetic insulating state, resulting from the synergic action of oxygen-vacancy ordering, lattice relaxation and spin interaction has been reported in the thin film of LaCoO_3 .⁴⁴

To further clarify the origin of this unusual evolution of conductivity, repeated resistance measurements at a single temperature point were performed in both in-plane directions. Fig. 6(a) shows the relative changes in resistance *versus* the number of repeated measurements, n_r , at 50 K. An increase of the resistance (up to more than 25%) is observed at the [100] direction, corroborating the important role of the current effect in the variation of conductivity. More interestingly, however, the resistance approaches a constant after several

repeated measurements ($n \geq 4$), unlike the case of repeated measurements with temperature cycling where the overall resistance increases continuously. This result indicates that the individual current effect cannot totally account for the observed conductivity variation. To fully understand the origin of the unusual conductivity transformation, the role of temperature cycling should also be considered. To verify such an assumption, further experiments were performed: three purely temperature cycles without the application of an electric current were inserted between normal repeated measurements of the temperature-dependent resistance. The measured results at the [01–1] direction are plotted in Fig. 6(b). One could find that the increased amount of the overall resistance after 3 extra temperature cycles is markedly larger than those between neighboring repeated measurements without extra temperature cycling in between. This result exemplifies that temperature cycling is indispensable in this novel conductivity transformation. Although the exact mechanism of temperature cycling in the evolution of conductivity is unclear at the moment, one could expect that the lattice changes induced by the temperature variation may contribute to the accumulation of oxygen vacancies by reducing its forming or/and migration energy.^{40,41,45,46} It's patently obvious that both the current effect and the temperature cycling have their own specific role in oxygen vacancy formation and neither of them can be dispensed in the observed novel conductivity transformation. Anyway, our present results have shown that oxygen vacancies could be introduced into the LSCO film simply by utilizing the combined current effect and temperature cycling below room temperature. Moreover, the concentration of oxygen vacancies in the LSCO film could be well regulated by adjusting the combination of the current effect and temperature cycling. Compared with the general route of annealing at high temperature in a reducing atmosphere, this newly developed oxygen defect engineering project is novel and highly effective.

It is worthwhile to note that the development of insulating conduction is different for two in-plane directions. One can

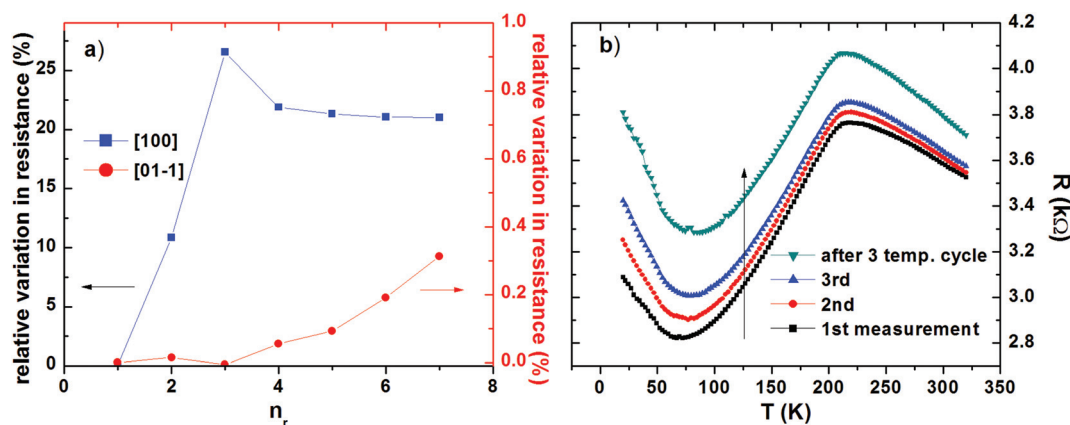


Fig. 6 (a) The relative changes in resistance *versus* number of repeated measurement for both in-plane directions of the LSCO/PMN-PT film at 50 K. (b) Repeated temperature-dependent resistance measurements along the [01–1] direction with 1 μA combined with purely temperature cycling without the application of an electric current.

find from Fig. 4(a) that the metallic conduction area for the [100] direction (blue shadow region) is much smaller than the one for the [01–1] direction (red shadow region). Accordingly, the vanishing point of both metal–insulator transitions appears earlier in the [100] direction (the passing point for curves of T_{MI1} and T_{MI2} , $n \sim 35$ for [100] and $n \sim 65$ for [01–1]). Moreover, the resistivity at an individual temperature along the [100] direction increases much faster with the number of repeated measurements than the one along the [01–1] direction (see Fig. 6(a)). These results indicate that the accumulation of oxygen vacancies and thus the transformation of Co^{4+} to Co^{3+} are much easier in the [100] direction, which could be ascribed to the anisotropic in-plane lattice strain-field in the LSCO/PMN-PT film. Previous research^{40,41,45} has shown that the tensile strain can lower the oxygen vacancy formation energy by increasing the ionic radius associated with the reduction reactions in the expanded lattice. Meanwhile, the larger tensile strain weakens orbit hybridization and charge transfer between the O-atom and the neighboring Co-atom, leading to a smaller formation and migration energy of the oxygen vacancy. As a result, the oxygen deficiencies can be formed more easily in the [100] direction, leading to the quick decrease of the $\text{Co}^{4+}/\text{Co}^{3+}$ ratio and thus the quick transformation from metallicity to insulativity in the [100] direction. Moreover, repeated transport measurements were also performed on the bulk sample of $\text{La}_{0.7}\text{Sr}_{0.3}\text{CoO}_3$. No obvious change of transport properties was observed after repeated measurements (see Fig. S3 in the ESI†), demonstrating that no conductivity transformation caused by the current effect assisted with temperature cycling occurs in the bulk sample. Obviously, such distinct conductivity response to the temperature cycling-assisted current effect in bulk and the thin film of LSCO should be closely relative to the tensile strain in the thin film, evidencing the important role of the lattice strain in oxygen vacancy formation.

Conclusions

We present the first experimental observation for oxygen defect engineering by the combined current effect and temperature cycling in cobaltite films. A continuous conductivity transformation from metallicity to insulativity was observed in the (011)-oriented LSCO/PMN-PT film during repeated measurements of the temperature-dependent transport properties. Further experiments demonstrated that the oxygen vacancies induced by the combined current effect and temperature cycling in the repeated measurements should be the main cause for the conductivity transformation. Meanwhile, it was found that the oxygen vacancy concentration in the film could be well regulated by adjusting the combination of the current effect and temperature cycling. Our work reveals a novel and highly effective method to introduce oxygen vacancies in the perovskite-type oxide $\text{La}_{1-x}\text{Sr}_x\text{CoO}_3$ film and provides a new avenue to design highly efficient catalysts.

Conflicts of interest

There are no conflicts to declare.

Acknowledgements

The authors acknowledge Beamline BL08U1A in Shanghai Synchrotron Radiation Facility (SSRF) for XAS measurements. This work was supported by the National Key Research and Development Program of China (Grant No. 2017YFA0303601, 2017YFB0702702, 2014CB643700, 2016YFB0700903 & 2016YFA0300701), the National Natural Sciences Foundation of China (Grant No. 11474341, 51531008, 11674378 and 51590880), the Key Program and Strategic Priority Research Program (B) of the Chinese Academy of Sciences.

Notes and references

- 1 M. A. Peña and J. L. G. Fierro, *Chem. Rev.*, 2001, **101**, 1981.
- 2 J. Maier, *Nat. Mater.*, 2005, **4**, 805.
- 3 J. K. Nørskov, T. Bligaard, J. Rossmeisl and C. H. Christensen, *Nat. Chem.*, 2009, **1**, 37.
- 4 Z. Shao and S. M. A. Haile, *Nature*, 2004, **431**, 170.
- 5 W. Liu and M. Flytzanistephanopoulos, *J. Catal.*, 1995, **153**, 317.
- 6 S. Royer and D. Duprez, *ChemCatChem*, 2011, **3**, 24.
- 7 S. Royer, D. Duprez, F. Can, X. Courtois, C. Batiot-Dupeyrat, S. Laassiri and H. Alamdari, *Chem. Rev.*, 2014, **114**, 10292.
- 8 D. N. Mueller, M. L. Machala, H. Bluhm and W. C. Chueh, *Nat. Commun.*, 2015, **6**, 6097.
- 9 X. Wang, K. Huang, W. Ma, Y. Cong, C. Ge and S. Feng, *Chem. – Eur. J.*, 2017, **23**, 1093.
- 10 A. Grimaud, K. J. May, C. E. Carlton, Y.-L. Lee, M. Risch, W. T. Hong, J. Zhou and Y. Shao-Horn, *Nat. Commun.*, 2013, **4**, 2439.
- 11 J. Suntivich, H. A. Gasteiger, N. Yabuuchi, H. Nakanishi, J. B. Goodenough and Y. Shao-Horn, *Nat. Chem.*, 2011, **3**, 546.
- 12 M. Søgaard, P. V. Hendriksen and M. Mogensen, *J. Solid State Chem.*, 2007, **180**, 1489.
- 13 E. L. Brosha, B. W. Chung, F. H. Garzon, I. D. Raistrick, R. J. Houlton and M. E. Hawley, *J. Electrochem. Soc.*, 1995, **142**, 1702.
- 14 P. Wang, L. Yao, M. Wang and W. Wu, *J. Alloys Compd.*, 2000, **311**, 53.
- 15 M. Imamura, N. Matsubayashi and H. Shimada, *J. Phys. Chem. B*, 2000, **104**, 7348.
- 16 Z. Cai, Y. Kuru, J. W. Han, Y. Chen and B. Yildiz, *J. Am. Chem. Soc.*, 2011, **133**, 17696.
- 17 M. Itoh, I. Natori, S. Kubota and K. Motoya, *J. Phys. Soc. Jpn.*, 1994, **63**, 1486.
- 18 B. Liu, Y. Q. Wang, G. J. Liu, H. L. Feng, H. W. Yang, X. Y. Xue and J. R. Sun, *Phys. Rev. B: Condens. Matter*, 2016, **93**, 094421.

- 19 J. R. Sun, H. W. Yeung, H. Li, K. Zhao, H. N. Chan and H. K. Wong, *J. Appl. Phys.*, 2001, **90**, 2831.
- 20 L. Borovskikh, G. Mazo and E. Kemnitz, *Solid State Sci.*, 2003, **5**, 409.
- 21 P. Pasierb, S. Komornicki and M. Rekas, *J. Phys. Chem. Solids*, 1999, **60**, 1835.
- 22 J. B. Goodenough and J. M. Longo, *Landolt Börnstein*, Springer, 1970, vol. III/4a.
- 23 J. Mizusaki, S. Yamauchi, K. Fueki and A. Ishikawa, *Solid State Ionics*, 1984, **12**, 119.
- 24 S. Wang, J. Yoon, G. Kim, D. Huang, H. Wang and A. J. Jacobson, *Chem. Mater.*, 2010, **22**, 776.
- 25 R. Caciuffo, D. Rinaldi, G. Barucca, J. Mira, J. Rivas, M. A. Señarís-Rodríguez, P. G. Radaelli, D. Fiorani and J. B. Goodenough, *Phys. Rev. B: Condens. Matter*, 1999, **59**, 1068.
- 26 Y. Y. Zhao, H. W. Yang, Y. Liu, H. Kuang, M. Zhang, W. L. Zuo, J. Wang, F. X. Hu, J. R. Sun and B. G. Shen, *IEEE Trans. Magn.*, 2015, **51**, 2100804.
- 27 Z. Othmen, A. Schulman, K. Daoudi, M. Boudard, C. Acha, H. Roussel, M. Oueslatia and T. Tsuchiya, *Appl. Surf. Sci.*, 2014, **306**, 60.
- 28 H. W. Yang, H. R. Zhang, Y. Li, S. F. Wang, X. Shen, Q. Q. Lan, S. Meng, R. C. Yu, B. G. Shen and J. R. Sun, *Sci. Rep.*, 2014, **4**, 6206.
- 29 A. D. Rata, A. Herklotz, K. Nenkov, L. Schultz and K. Dörr, *Phys. Rev. Lett.*, 2008, **100**, 076401.
- 30 M. A. Señarís-Rodríguez and J. B. Goodenough, *J. Solid State Chem.*, 1995, **118**, 323.
- 31 S. P. Cramer, F. M. F. de Groot, Y. Ma, C. T. Chen, F. Sette, C. A. Kipke, D. M. Eichhorn, M. K. Chan and W. H. Armstrong, *J. Am. Chem. Soc.*, 1991, **113**, 7937.
- 32 M. Merz, P. Nagel, C. Pinta, A. Samartsev, H. v. Löhneysen, M. Wissinger, S. Uebe, A. Assmann, D. Fuchs and S. Schuppler, *Phys. Rev. B: Condens. Matter*, 2010, **82**, 174416.
- 33 D. Fuchs, M. Merz, P. Nagel, R. Schneider, S. Schuppler and H. von Löhneysen, *Phys. Rev. Lett.*, 2013, **111**, 257203.
- 34 M. Abbate, F. M. F. de Groot, J. C. Fuggle, A. Fujimori, O. Strebel, F. Lopez, M. Domke, G. Kaindl, G. A. Sawatzky, M. Takano, Y. Takeda, H. Eisaki and S. Uchida, *Phys. Rev. B: Condens. Matter*, 1992, **46**, 4511.
- 35 D. Mierwaldt, S. Mildner, R. Arrigo, A. Knop-Gericke, E. Franke, A. Blumenstein, J. Hoffmann and C. Jooss, *Catalysts*, 2014, **4**, 129.
- 36 M. Belli, A. Scafati, A. Bianconi, S. Mobilio, L. Palladino, A. Reale and E. Burattini, *Solid State Commun.*, 1980, **35**, 355.
- 37 C. Rossel, A. Rosová, K. Hušková, D. Machajdík and K. Fröhlich, *J. Appl. Phys.*, 2006, **100**, 044501.
- 38 L. Yao, S. Inkinen and S. van Dijken, *Nat. Commun.*, 2017, **8**, 14544.
- 39 N. Manca, L. Pellegrino and D. Marré, *Appl. Phys. Lett.*, 2015, **106**, 203502.
- 40 U. Aschauer, R. Pfenninger, S. M. Selbach, T. Grande and N. A. Spaldin, *Phys. Rev. B: Condens. Matter*, 2013, **88**, 054111.
- 41 C. Becher, L. Maurel, U. Aschauer, M. Lilienblum, C. Magén, D. Meier, E. Langenberg, M. Trassin, J. Blasco, I. P. Krug, P. A. Algarabel, N. A. Spaldin, J. A. Pardo and M. Fiebig, *Nat. Nanotechnol.*, 2015, **10**, 661.
- 42 N. Biškup, J. Salafranca, V. Mehta, M. P. Oxley, Y. Suzuki, S. J. Pennycook, S. T. Pantelides and M. Varela, *Phys. Rev. Lett.*, 2014, **112**, 087202.
- 43 J. Okamoto, H. Miyauchi, T. Sekine, T. Shidara, T. Koide, K. Amemiya, A. Fujimori, T. Saitoh, A. Tanaka, Y. Takeda and M. Takano, *Phys. Rev. B: Condens. Matter*, 2000, **62**, 4455.
- 44 N. Biškup, J. Salafranca, V. Mehta, M. P. Oxley, Y. Suzuki, S. J. Pennycook, S. T. Pantelides and M. Varela, *Phys. Rev. Lett.*, 2014, **112**, 087202.
- 45 R. U. Chandrasena, W. Yang, Q. Lei, M. U. Delgado-Jaime, K. D. Wijesekara, M. Golalikhani, B. A. Davidson, E. Arenholz, K. Kobayashi, M. Kobata, F. M. F. de Groot, U. Aschauer, N. A. Spaldin, X. Xi and A. X. Gray, *Nano Lett.*, 2017, **17**, 794.
- 46 M. Kubicek, Z. Cai, W. Ma, B. Yildiz, H. Hutter and J. Fleig, *ACS Nano*, 2013, **7**, 3276.